Targeting NUPR1 with the small compound ZZW-115 is an efficient strategy to treat hepatocellular carcinoma

Wenjun Lan, Patricia Santofimia-Castaño, Yi Xia, Zhengwei Zhou, Can Huang, Nicolas Fraunhoffer, Dolores Barea, Melchiore Cervello, Lydia Giannitrapani, Giuseppe Montalto, et al.

Version of Record: https://www.sciencedirect.com/science/article/pii/S0304383520302263
Manuscript_f0bc440b958182645f990904f514f151

Targeting NUPR1 with the small compound ZZW-115 is an efficient strategy to treat hepatocellular carcinoma

Wenjun Lan[1,2,#], Patricia Santofimia-Castaño[1,#], Yi Xia[3], Zhengwei Zhou[3], Can Huang[1], Nicolas Fraunhoffer[1], Dolores Barea[1], Melchiore Cervello[5], Lydia Giannitrapani[6], Giuseppe Montalto[6], Ling Peng[2], Juan Iovanna[1*]

[1]Centre de Recherche en Cancérologie de Marseille (CRCM), INSERM U1068, CNRS UMR 7258, Aix-Marseille Université and Institut Paoli-Calmettes, Parc Scientifique et Technologique de Luminy, 163 Avenue de Luminy, 13288 Marseille, France.

[2]Aix-Marseille Université, CNRS, Centre Interdisciplinaire de Nanoscience de Marseille, UMR 7325, «Equipe Labellisée Ligue Contre le Cancer», Parc Scientifique et Technologique de Luminy, 163 Avenue de Luminy, 13288 Marseille, France.

[3]Chongqing Key Laboratory of Natural Product Synthesis and Drug Research, School of Pharmaceutical Sciences, Chongqing University, No.55 Daxuecheng South Road, Chongqing 401331, P. R. China.

[4]Consejo Nacional de Investigaciones Científicas y Técnicas. Centro de Estudios Farmacológicos y Botánicos (CEFYBO). Facultad de Medicina. Buenos Aires, Argentina.[5]Consiglio Nazionale Delle Ricerche, Istituto per la Ricerca e l'Innovazione Biomedicale (IRIB), Palermo, Italy.

[6]Dipartimento di Promozione della Salute, Materno-Infantile, Medicina Interna e Specialistica di Eccellenza (PROMISE), University of Palermo, Palermo, Italy.

[#]denotes equal contribution

*Corresponding author address: Juan Iovanna, email: juan.iovanna@inserm.fr Centre de Recherche en Cancérologie de Marseille (CRCM), INSERM U1068, CNRS UMR 7258, Aix-Marseille Université and Institut Paoli-Calmettes, Parc Scientifique et Technologique de Luminy, 163 Avenue de Luminy, 13288 Marseille, France. Phone +33-491828803; Mobil Phone +33-760988158; Fax +33-491 826083.

Abstract

HCC is a highly lethal malignancy with Sorafenib as the only molecularly targeted drug. The multifunctional stress-associated protein, NUPR1, plays an essential role in controlling cell growth, migration, invasion and Sorafenib resistance in HCC. We report here that NUPR1 expression is absent in healthy liver and it is progressively upregulated in HCC premalignant lesions such as hepatitis and cirrhosis with a maximum expression in HCC samples, highlighting that NUPR1 is a potential drug target for HCC. We therefore assessed in this work, ZZW-115, a strong inhibitor of NUPR1, as a promising candidate for the treatment of HCC. We validated its extraordinary antitumor effect on HCC by using two HCC cell lines, HepG2- and Hep3B, both in cell based experiments and xenografted mice. We further revealed that ZZW-115 treatment induced cell death by apoptosis and necroptosis mechanisms, with a concomitant mitochondrial metabolism failure that triggers lower ATP production. Furthermore, the ATP depletion cannot be rescued by the apoptosis inhibitor Z-VAD-FMK and/or the necrosis inhibitor Necrostatin-1, indicating that ZZW-115 induces cell death through the mitochondrial failure.

INTRODUCTION

Hepatocellular carcinoma (HCC) is the most common primary liver malignancy and the sixth cause of cancer-related death worldwide, affecting particularly the population of Eastern Asia and sub-Saharan Africa [10, 21]. Although the incidence and mortality is continuously increasing, slight progress towards the improvement of the HCC therapies has been achieved. Among all the therapies, Sorafenib is the only FDA approved targeted therapy against advanced HCC as a multikinase inhibitor [4]. Unfortunately, Sorafenib has modest benefits, with a low response rate and a limited improvement in median overall survival, with only of 2-3 months as a sole treatment, being ineffective as an adjuvant after curative resection. Clearly, new therapeutic drug and targets for treating HCC are urgently needed. Previously, it has been reported a strong linkage between HCC and the activation of the multifunctional stress-associated protein NUPR1 (Nuclear Protein 1). Over-expression of NUPR1 in hepatitis B participates in HCC development in a SMAD4-dependent manner [2]. Also, NUPR1 expression is upregulated by triiodothyronine/thyroid hormone receptor (T3/TR) signaling cascade, which in turn activates transcription of the PDGFA and MEK/ERK activation to induce endothelial cell angiogenesis *in vitro* and *in vivo* [6]. The work of Ji *et al.* demonstrated that the serum from chronic hepatitis B patients promotes growth and proliferation of HCC cells, enhancing NUPR1 expression via the IGF-II/IGF-IR/MEK/ERK signaling pathway [12]. Beside hepatitis, nonalcoholic steatohepatitis (NASH) is another leading cause of HCC, however, the molecular pathogenesis and the mechanisms involved in this progression are not fully understood. De Conti and colleagues demonstrated in an animal model, that resembles the human NASH-related HCC, a strong reduction of the H4K16 acetylation. This event is a key pathophysiologic mechanism that contributes to the development of NASH-derived HCC and that is controlled by the overexpression of NUPR1. Mechanistically, NUPR1 inhibits the histone acetylase KAT8, which initiates the deacetylation of histone H4K16 [8]. Lastly, it was suggested that the mitochondrial defects systematically observed in HCC are responsible of the NUPR1-granulin pathway activation in a Ca^{2+} signaling-dependent manner [13, 14]. Altogether we can assume that NUPR1 expression is systematically activated in precancerous and cancerous tissues by several concomitant pathways. Therefore, NUPR1 should be considered as a promising therapeutic target. In this way, genetic inactivation of NUPR1 on HCC-derived cells by using RNA interference methods is an efficient approach to inhibit the proliferation both *in vitro* and *in vivo* [3, 9, 11], migration and invasion [9, 11] and to improves Sorafenib anticancer effect [6, 9]. Unfortunately, genetic approaches like RNA interference cannot be used in clinics for the moment. We have been therefore working for the alternative solution to develop small molecular inhibitors to target NUPR1 in the view to develop novel and potent drug candidates for treating HCC.

It is to note that NUPR1 is a nuclear intrinsically disordered protein (IDP), which is extremely difficult to target by drug discovery program using conventional methods. We have inventively developed a multidisciplinary approach combining biological, biochemical,

bioinformatics and biophysical methods to screen the inhibitor candidates against NUPR1. One of lead compounds named ZZW-115 shows the most potent capacity to interact with NUPR1 [15, 18, 19], constituting a promising anticancer candidate. Supporting this hypothesis, we recently demonstrated that ZZW-115 strongly inhibited tumor growth in pancreatic ductal adenocarcinoma (PDAC) mice models [19].

As ZZW-115 is a powerful inhibitor against NUPR1, we therefore reasoned that ZZW-115 could also be a promising candidate for the treatment of other cancers which overexpress NUPR1, such as HCC. In this work, we validated the antitumor effect of ZZW-115 on HCC by using both cell and animal models. In our mechanistic analysis, we noticed the induction of a programmed cell death by both necroptosis and apoptosis after ZZW-115 treatment, with a strong mitochondrial metabolism loss, which results in a huge reduction of ATP content. Necrostatin-1 and Z-VAD-FMK, inhibitors of necroptosis and apoptosis, respectively, were able to inhibit the cell death induced by ZZW-115, but not to rescue the mitochondrial activity. Taken together, our results suggest that ZZW-115 constitutes a promising drug candidate for HCC patients by targeting NUPR1.

MATERIAL AND METHODS

Cell viability assays

Cell viability after treatment was assessed in the following HCC cancer cell lines: HepG2 and Hep3B. Cells were obtained from ATCC and maintained in DMEM (Invitrogen) supplemented with 10% FBS at 37°C with 5% CO_2. Cells were plated in 96-well plates (5000 cells/well) at the first day. After overnight culture, cell medium was replaced with 0-100 µM concentration of the ZZW-115 in the second day. After 72 h drug treatment, PrestoBlue (Thermo Fisher) was used to measure the cell viability for 3 h, according to the protocol provided by the supplier. Cell viability was normalized to untreated cell rates.

Immunohistochemistry (IHC) assays

This study included 24 primary liver samples from patients with hepatitis virus B (HBV) (n=6), chronic cirrhosis associated (n=6), HCC (n=6) and normal liver (n=6) (14 male, 10 females; mean age 53 years, range 38-69 years. All patients had in fact undergone surgery at the Division of Surgery of the University Medical School of Palermo, Italy, Palermo, Italy. Informed consent was obtained from all patients. The study protocol is conformed to the ethical guidelines of the 1975 Declaration of Helsinki.

IHC detection of NUPR1 protein was carried out on 5-µm-thick deparaffinized sections. Tissue sections were rehydrated by a series of graded ethanol concentration. The antigen unmasking technique was performed using citrate buffer pH 6 (Diapath)/Tween 0.05%. Endogenous peroxidase activity was quenched with 3% (vol/vol) H_2O_2 for 15 minutes, which

was followed by blocking nonspecific protein binding using 5% bovine serum albumin (BSA) in phosphate-buffered saline (PBS) for 30 minutes at 37°. Subsequently, the samples were incubated overnight at 4°C with the anti-NUPR1 home-made polyclonal rabbit antibody previously described [17] (1/200; pH 6). Staining was revealed by the Vectastatin ABC kit (PK-4001, Vector Laboratories) for 30 minutes following manufacturer's instructions, counterstained with hematoxylin (Sigma), dehydrated, and mounted. For the negative controls, rabbit antiserum was substituted for the NUPR1 antibody. All the sections were analyzed and examined in an Eclipse 90i Nikon microscope (Nikon Instruments Europe B.V., Champigny-sur-Marne, France). The relative percentages of positive nuclei for NUPR1 were evaluated by Image J (Fiji) software.

Cohort Validation and Survival analysis

RNA expression data for 421 patients was downloaded using TCGAbiolinks R package (10.1093/nar/gkv1507) from the Cancer Genome Atlas Liver Hepatocellular Carcinoma project (TCGA-LIHC), and the expression values were log2 transformed and normalized with edgeR R package (10.1093/bioinformatics/btp616). The TCGA cohort was composed of 12% peritumoral normal tissue (n=50) and 88% primary HCC (n=371). Kaplan-Meier survival analysis with the log-rank test was performed by the R packages survival (10.1007/978-1-4757-3294-8).

Immunofluorescence staining of tumor samples

Immunofluorescence staining was performed on 5-µm-thick paraffin-embedded tissue sections. The following antibodies were used: anti-Ki67 (#ab 92742, Abcam) and anti-cleaved Caspase-3 (#9661; Cell Signaling Technology, Inc.). DAPI (D1306) was from Thermo Fisher scientific). Primary antibodies were diluted 1:200 and secondary antibody Goat anti-Rabbit IgG (H+L) Alexa Fluor 488, # A27034 from Thermo Fisher scientific) 1:500. The incubations were performed at room temperature. Signals were detected with a LSM 880 controlled by Zeiss Zen Black, 63x lens. The calculation of positives cells was performed by Image J (Fiji) software.

Animals

Female CAnN.Cg-Foxn1nu/Crl BALB/c nude mice were provided by Charles River Laboratories. Mice were kept within the Experimental Animal House of the Centre de Cancérologie de Marseille, pôle Luminy (Centre de Recherche en Cancérologie de Marseille). Five million of HepG2 or Hep3B HCC cells were inoculated subcutaneously in nude mice (5 weeks old) and they were separated into 3 (HepG2-injected) or 2 (Hep3B-injected) groups of 5 subjects each. Mice were treated daily with 0.5% DMSO in physiologic serum (vehicle), 2.5 mg/kg or 5 mg/kg of ZZW-115 when the tumor volume reached 200 mm^3. Every 3 or 5 days, the mice were weighed and the tumor volumes were measured. Mice were sacrificed after 20 days of treatment.

LDH assay, ATP production, and caspase-3/7 activity assay

HepG2 and Hep3B cells were seeded at a density of 10,000 cells per well in 96-well plates. Cells were allowed to attach overnight and treated the next day for 24 h with ZZW-115 alone or in combination with Necrostatin-1 (40 μM) and/or Z-VAD-FMK (20 μM) (both from Sigma). At the end of the experiment, LDH release, ATP production, and caspase-3/7 activity were monitored using CytoTox-ONE (#G7890 Promega), CellTiter-Glo (#G7571 Promega) and Caspase-Glo 3/7assay (#G8091 Promega), respectively. Data were normalized to the cell number.

OXPHOS and glycolytic metabolism

Measurements were performed using a Seahorse Bioscience XF24 Extracellular Flux Analyzer (Agilent). This system allowed measurement of the cellular oxygen consumption rate (OCR, in pmoles/min) and the extracellular acidification rate (ECAR in mpH/min). 30,000 cells/well were plated and were allowed to attach overnight. Next day, HCC cells treated with ZZW-115 alone or in combination with Z-VAD-FMK and/or Necrostatin-1 for 8 or 24 h. OCR was measured using the XF Cell Mito Stress Test Kit (Agilent) under basal conditions, and in response to 1 μM oligomycin and 0.25 or 0.5 μM of carbonylcyanide p-(trifluoro-methoxy) phenylhydrazone (FCCP) in Hep3B or HepG2, respectively. Oligomycin injection allowed calculation of the OCR for ATP production, and FCCP treatment gave two indexes; the maximal OCR capacity and the spare respiratory capacity. Finally, OCR was stopped by adding the electron transport chain inhibitors rotenone and antimycin A (0.5 μM each). ECAR was measured using the Seahorse XF Glycolysis Stress Test Kit. Glycolysis was calculated as the difference between the values of ECAR upon glucose addition (10 mM) and basal ECAR. Glycolytic capacity was calculated as the difference between ECAR following the injection of 1 μm oligomycin, and the basal ECAR. Finally, glycolytic reserve was calculated as the difference in ECAR between glucose and oligomycin injections. At the end of the experiment, glycolysis was stopped by adding 2-Deoxyglucose (100 mM). Levels of OCR and ECAR were normalized to the cell number.

AnnexinV/PI staining

Cell were collected after 12 h treatment with ZZW-115 alone or in combination with Z-VAD-FMK and/or Necrostatin-1. HCC cells were detached with Accutase (Gibco, Life Technologies), washed once with PBS, and resuspended in 100 μL of Annexin-binding buffer. Pacific-Blue Annexin V (5 μl, BioLegend) and propidium iodide (5 μl, Miltenyi Biotec) were added to the cell suspension and incubated for 15 minutes. Then, 400 μl of 1x Annexin-binding buffer was added to each sample. MACSQuant-VYB (Miltenyi Biotec) device was used to collect 10,000 events per sample. Data analysis was performed using FlowJo software.

Mitochondrial membrane potential

Measurement was performed using the MITO-ID Membrane potential detection kit (ENZ-51018) according to the manufacturer's protocol. Briefly, cells were collected, washed, and

preincubated in 500 µl of the Assay Solution containing 5 µl of MITO-ID MP Detection Reagent for 15 min. After this, 10,000 events per sample were collected in a MACSQuant-VYB and orange fluorescence data analysis was performed using the FlowJo software. Median of the fluorescence is shown.

ADP/ATP Ratio

Measurement was performed using the ADP/ATP Ratio Assay Kit (MAK135 form Sigma-Aldrich). Briefly, 5000 cells/well were seeded in a 96 well plate. Cells were allowed to attach overnight and treated the next day for 24 h with ZZW-115 at increasing concentrations. ATP and ADP were measured on a luminometer and the ratio ADP/ATP was calculated following manufacturer's instructions.

Statistics

Statistical analyses were performed by using the unpaired 2-tailed Student t test, 1-way ANOVA with Tukey's post hoc test, or 2-way ANOVA with Bonferroni's post hoc test was used when appropriate. IC_{50} and area under the curve (AUC) values were calculated by nonlinear regression curves with robust fit using GraphPad software. Values are expressed as mean ± SEM. Wilcoxon rank sum test for NUPR1 expression levels was performed with R basic functions. Data are representative of at least 3 independent experiments with technical triplicates completed. A P value less than 0.05 was considered significant.

Study approval

All experimental protocols were carried out in accordance with the nationally approved guidelines for the treatment of laboratory animals. All experimental procedures on animals were approved by the Comité d'éthique de Marseille numéro 14 (C2EA-14).

RESULTS

NUPR1 expression is increasing according to the human liver disease progression

Approximately 70%-90% of patients with HCC have an established background of chronic liver disease and cirrhosis. The major risk factors for developing cirrhosis are chronic infection with hepatitis B virus (HBV), hepatitis C virus (HCV), alcoholic liver disease, and NASH. In order to study the evolution of NUPR1 expression in different stages of liver diseases we investigated NUPR1 expression in normal liver (n=6), in liver with hepatitis (n=6), in cirrhotic liver (n=6) and in HCC (n=6) by immunohistochemistry (Figure 1A). Demographic features and clinical parameters of the patients are presented in Table 1. The immunohistochemical analysis showed that NUPR1 expression is closely related to the evolution of liver diseases. Whereas healthy livers showed almost completely negative staining, NUPR1 expression increases progressively from liver hepatitis, liver cirrhosis up to

HCC. In addition, NUPR1 staining was located almost exclusively in the nucleus of hepatocytes. Quantification of staining showed that liver with hepatitis presents 34% of positive nuclei, with cirrhosis 50% and with HCC 93%, as showed in Figure 1B.

To validate the relation of NUPR1 to the progression of liver diseases, we analyzed the expression of NUPR1 in a TCGA cohort (n=421). NUPR1 levels were significantly higher in HCC than peritumoral tissue (p value < 0.0001; Figure 1C). Furthermore, Kaplan–Meier survival analysis revealed a strong negative association among NUPR1 expression and clinical outcome (Figure 1D). Patients with high NUPR1 had overall survival (OS) median of 1423 days, whereas low NUPR1 patient' OS median is 2456 days (p value = 0.0053).

HCC cell lines are sensitive to ZZW-115-treatment *in vitro* and *in vivo*

Because NUPR1 is highly expressed in HCC, we tried to study the effect of the NUPR1 inhibitor ZZW-115 on two HCC-derived cell lines, HepG2 and Hep3B, 72h post-treatment. Remarkably, ZZW-115 exhibited strong inhibition on the proliferation of HepG2 and Hep3B cell lines, with IC_{50} values being 0.97 ± 0.27 μM and 3.31 ± 0.40 μM, respectively (Figure 2). HepG2 is more sensitive to the ZZW-115 treatment than Hep3B, although ZZW-115 is effective for both cell lines.

Since ZZW-115 showed a strong anti-cancer activity in both HCC cell lines *in vitro*, we decided to further analyze its effect *in vivo*. To achieve this goal, ZZW-115 anti-cancer effects were tested using HepG2 cells xenograft mice model by injecting 5 x 10^6 cells. When the tumors attained a volume of around of 200 mm^3, the mice were separated in three groups. Two different doses (2.5 mg/kg or 5.0 mg/kg) of ZZW-115 were daily injected, whereas the control group was treated with the same volume of vehicle solution. As expected, tumors size from control group grew rapidly, but in treated groups increased much less (when treated with 2.5 mg/kg) or even decreased (when treated with 5.0 mg/kg) compared to control group. Clearly, a dose dependent effect was observed. Whereas the tumor volume of the control group increased from 247.84 ± 33.79 mm^3 to 1396.84 ± 124.17 mm^3, the tumor size of the group treated with 2.5 mg/kg grew from 253.30 ± 32.20 mm^3 to 550.66 ± 262.22 mm^3 and decreased from 196.20 ± 16.41 mm^3 to 135.52 ± 35.97 mm^3 in the group treated with 5.0 mg/kg (Figure 3A). Remarkably, the tumors volume of all mice treated with higher dose of ZZW-115 decreased immediately after starting the injections and became almost undetectable after 20 days of treatment.

To further validate the antitumor effect of ZZW-115, we tested the compound on Hep3B HCC cells xenografted in mice. Tumors were obtained by subcutaneous injection of 5 x 10^6 cells. On this model we used a dose of 5 mg/kg of ZZW-115 for the treatment which was started when tumors attained about 200 mm^3 for 20 days. As expected, in control group the tumor size was progressively increased from 225.48 ± 13.16 mm^3 to 1733.10 ± 241.97 mm^3. Contrarily, after the daily treatment with 5 mg/kg ZZW-115, mice tumors size did not grow,

remaining almost the same during the treatment (from 215.72 ± 5.49 mm^3 to 323.64 ± 51.59 mm^3) (Figure 3B).

ZZW115 induced apoptosis and antiproliferative effect *in vivo*

To reveal the molecular mechanisms of ZZW-115 anticancer effect on HCC tumors, we preformed immunofluorescence staining for detecting the cleaved caspase 3 and Ki67. Our aim was to measure apoptosis and antiproliferative effects on samples obtained at the end of the treatment of xenografted-mice. As shown in Figure 3C and D, tumors induced with HepG2 cells show a strong increase in the quantity of cells with activated caspase 3 after the treatment with ZZW-115 (1.72 ± 0.21 vs 91.27 ± 0.45; p value <0.0001). A similar result was obtained with the xenograft produced with the Hep3B cells (1.56 ± 0.20 vs 80.55 ± 0.35; p value <0.0001). Contrarily, tumors induced with HepG2 cells shows a strong decrease in Ki67 positive cells in tumors treated with ZZW-115 (51.69 ± 0.61 vs 2.01 ± 0.26; p value <0.0001) and we observed similar results in tumors produced with Hep3B cells (61.68 ± 0.70 vs 3.62 ± 0.23; p value <0.0001). Altogether, our results demonstrated that treatment of HCC with ZZW-115 induces apoptosis and arrest of proliferation in xenografted-mice.

ZZW-115-induced cell death can be reverted by the pan-caspase inhibitor Z-VAD-FMK and the necroptosis inhibitor Necrostatin-1

In order to study whether ZZW-115 induced cell death by apoptosis and/or necroptosis, we used the flow cytometry analysis after co-labelling the cells with Annexin V and PI to measure apoptosis and necrosis respectively. HepG2 cells treated with ZZW-116 showed 37.00% ± 0.5 of Annexin V and propidium iodide (PI) positive cells as showed in Figure 4A and 5B. Co-treatment with Necrostatin-1 (an inhibitor of necroptosis) or Z-VAD-FMK (a pan-caspase inhibitor), alone or in combination, resulted in a significant reduction of cell death to 18.60% ± 0.6 (p value = 0.007), 17.05% ± 0.15 (p value = 0.008) and 13.8% ± 0.7 (p value = 0.002) respectively. Concordantly, treatment of Hep3B cells with ZZW-115 shows 73.83% ± 0.93 % of Annexin V and PI positive cells as presented in Figure 4A and 4B. When these cells were co-treated with Necrostatin-1 or Z-VAD-FMK, alone or together, cell death was significantly reduced to 25.33% ± 0.71 (p value <0.0001), 26.70% ± 0.90 (p value <0.0001) and 17.8% ± 0.4 (p value <0.0001), respectively. In order to confirm that ZZW-115 induces apoptosis and necroptosis, we further measured caspase 3/7 activity and LDH release (Figure 4C and 4D). In agreement with the flow cytometry data, ZZW-115 was able to increase caspase activity and LDH release in HepG2 and Hep3B cells in a dose dependent manner. Moreover, pre-incubation with Necrostatin-1 or Z-VAD-FMK were able to reduce significantly the activation of each cell death pathway, as well as in combination (Figure 4C and 4D). These results strongly suggest that ZZW-115 treatment of HCC cells induced apoptosis and necroptosis concomitantly.

ZZW-115-treatment induces metabolic failure

Changes in the intracellular level of ATP are determinant of induction of cell death by necroptosis or apoptosis. ATP is one of the mayor regulator in the activation of the cell death pathways [16]. We measured the intracellular level of ATP in HepG2 and HepB3 cells after treatment with different concentrations of ZZW-115 (Figure 5A and Supplementary Figure 1A). Our data showed that the amount of ATP decreases in a concentration-dependent manner in both cell lines. Interestingly, co-treatment with Necrostatin-1 or Z-VAD-FMK, alone or together, was unable to reverse this effect.

As the major sources of ATP production are the mitochondrial OXPHOS and anaerobic glycolysis, we further performed metabolic studies by using the Seahorse device in ZZW-115-treated cells. After 8 h of treatment, we observed in both HCC cell lines, HepG2 (Figure 5B) and HepB3 (Supplementary Figure 1B), a significant decrease in mitochondrial metabolism. In fact, basal and maximal respiration capacities were highly decreased after treatment, accompanied with a reduced ATP production. Interestingly, co-treatment of the cells with Necrostatin-1 or Z-VAD-FMK alone or together was unable to reverse this mitochondrial metabolism failure. Importantly, after 24 h of treatment the mitochondrial defect was greater, as presented in Figures 5C and Supplementary Figure 1C, indicating that this injury is progressive and perhaps irreversible. In agreement with the mitochondrial function loss and the incapability of ATP production, we found a strong decrease of the mitochondrial membrane potential when the HCC were challenged with increasing concentrations of ZZW-115 (Figures 5D and Supplementary Figure 1D). Moreover, ZZW-115-treatment induced an increase of the ADP/ATP ratio on a concentration-dependent manner (Figure 5E and Supplementary Figure 1E) highlighting again the metabolic failure in the HCC cells. In addition, after 8 h of treatment we observed an important increase in glycolysis as expected during mitochondrial failure, in both HCC cells lines (Figure 5F and Supplementary Figure 1F). However, this mitochondrial switch of ATP production from OXPHOS to glycolysis was transitory since after 24 h of treatment glycolytic activity was strongly decreased, with stronger effect on Hep3B cells (Figure 5G and Supplementary Figure 1G). Glycolytic activity is known to be less profitable than OXPHOS in terms of ATP production, thus this switch towards glycolytic activity could compensate the ATP mitochondrial production loss for short terms, but not for sustained treatments. Like OXPHOS analysis, co-treatment with Necrostatin-1 or Z-VAD-FMK, alone or in combination, were unable to reverse this glycolytic switch (Figure 5F-G and Supplementary Figure 1F-G). Altogether, our results suggest that the mitochondrial failure induced by ZZW-115 treatment promoted a glycolytic switch which tried to compensate the loss of energy. Moreover, because the co-treatment with Necrostatin-1 and/or Z-VAD-FMK was unable to reverse the OXPHOS and glycolytic switch, we assume that cell death is downstream of the mitochondrial failure.

DISCUSSION

Worldwide, HCC is the sixth most prevalent cancer [10]. More than 600,000 people are newly diagnosed every year and approximately the same number dies due to HCC annually. The main etiology of HCC is liver cirrhosis, which is caused by chronic hepatitis B or C, alcohol consumption, fatty liver diseases, or less commonly, autoimmune or genetic metabolic liver diseases [5]. Medical therapies, including cytotoxic chemotherapies with single drugs (doxorubicin, gemcitabine, oxaliplatin, capecitabine) or the combination protocols such as PIAF, FOLFOX or ECF, has failed to improve overall survival in most clinical trials to date. More promising are the molecular targeted therapies represented by Sorafenib. Sorafenib is the only approved systemic agent for the treatment of advanced HCC. It is a multikinase inhibitor whose targets include Raf-1 and B-Raf serine/threonine kinases, vascular endothelial growth factor receptor (VEGFR) and platelet-derived growth factor receptor (PDGFR) tyrosine kinases, and c-kit receptors [20]. However, Sorafenib only shows modest benefits, with a low response rate and a limited improvement in median overall survival. It is therefore of timely importance to search for and identify novel therapeutic targets and drug candidates for treating HCC.

In this paper, we provide evidences that the multifunctional stress-associated protein NUPR1 constitutes alternative drug target for HCC, and ZZW-115, the powerful inhibitor of NUPR1, is a promising drug candidate for treating HCC. We revealed that NUPR1 expression is absent in healthy liver but it is progressively upregulated in HCC premalignant lesions, such as chronic hepatitis and cirrhosis, with a maximum expression in HCC samples. Moreover, these results were corroborated by analyzing in a TCGA cohort the expression of NUPR1, which was again significantly greater in tumoral tissue compared with the peritumoral one. Then, we demonstrated that treatment of HCC with the NUPR1 inhibitor ZZW-115 induced cell death *in vitro* and tumor growth arrest *in vivo.* Moreover, this anti-tumoral effect is driven by inducing cell death via both necroptosis and apoptosis, which can be inhibited by their corresponding inhibitors Necrostatin-1 and Z-VAD-FMK, respectively. Cell death occurs through a strong decrease in ATP intracellular concentration, as a default of the mitochondrial function which cannot be compensated by the glycolytic switch. Altogether, ZZW-115 is an extremely original drug candidate for HCC therapy.

NUPR1 is a promising therapeutic target in liver cancer because, on one hand, it is implicated in controlling cell growth, migration, invasion and Sorafenib resistance in liver cancer [6, 9, 11]. On the other hand, NUPR1 expression is progressively upregulated during liver diseases progression but it is absent in to normal liver (Figure 1A). Also RNA interference approaches directed to the genetic inactivation of *Nupr1* showed to be an efficient, although clinically unusable, method for treat HCC both *in vitro* and *in vivo* [3, 9, 11].

It was a great challenge to target NUPR1 because it is an intrinsically disordered protein (IDP) that lacks of a fixed or ordered three-dimensional structure for drug design. Nonetheless, we were able, by using a multidisciplinary approach, to find an original small compound, Trifluoperazine, able to bind and to inhibit NUPR1 activity [15, 18]. Furthermore, as expected

Trifluoperazine already showed antitumoral effect, inducing tumor grown decrease in orthotropic HCC mouse model [7]. However, although it showed an anticancer effect this treatment was accompanied by several neuroleptic side effects in our *in vivo* experiments. Then, we synthesized the ZZW-115 compound, which is structurally related to the Trifluoperazine, but it is around ten times more efficient as an anticancer agent and more important it is devoid of the neuroleptic side effect [19]. Accordingly, ZZW-115 demonstrated to be efficient for treating pancreatic ductal adenocarcinoma [19].

Here, we demonstrated that inhibition of NUPR1 by ZZW-115 can inhibit HCC tumor growth *in vivo* induced by HepG2 and Hep3B HCC-derived cells. Daily injection of 5 mg/kg promoted a total arrest of tumor growth. This anticancer effect was associated with a strong increase in activated caspase 3 staining, as a marker of apoptosis, and a strong decrease in Ki67 staining, used as a marker of tumor growth. Mechanistically, we demonstrated that ZZW-115 treatment induces necroptosis and apoptosis, which were reversed respectively by the treatment with Necrostatin-1 and Z-VAD-FMK alone or in combination. Cell death is induced because treatments with ZZW-115 decreased the intracellular level of ATP as consequence of a mitochondrial failure. An important point to be noted is that induction, by a drug like ZZW-115, of two concomitants cell death pathways in the same cell, such are necroptosis and apoptosis, is predictive of having greater anti-cancer effect. In this regard, cells may escape of one of these mechanisms but it is more difficult to develop resistance mechanisms against both necroptosis and apoptosis.

Furthermore, we found that ZZW-115 decreased ATP level in a dose-dependent manner. In order to study the relationship of ZZW-115 induced cell death and ATP level decline, we evaluated different mitochondrial parameters such as basal respiration, maximal respiration and the ATP production during OXPHOS after treatment with ZZW-115 and we found a collapse in these mitochondrial parameters. Also we observed a significant increase in the glycolytic activity of the cells, trying to compensate the ATP deficit. Interestingly, these changes were insensitive to Z-VAD-FMK and/or Necrostatin-1, indicating that mitochondrial failure is cause and not consequence of the cell death induced by ZZW-115. Previously, it has been reported that upregulation of the NUPR1 in HCC is a consequence of mitochondrial defects frequently observed in HCC cells [13, 14]. In this work, we describe that NUPR1 plays a major role in mitochondrial stability, since its inhibition induces dramatic respiratory defects originated in the mitochondria due to a mitochondrial membrane potential loss. Altogether, we can conclude that NUPR1 works upstream of the cellular respiration mechanism, but probably also downstream since NUPR1 expression is activated in response to mitochondrial failure.

Conclusion

To sum up, we demonstrated that a remarkable increase of NUPR1 occurs along with the HCC evolution process ZZW-115, a strong NUPR1 inhibitor, showed powerful anticancer effect in HCC in *in vitro* and *in vivo*. We highlighted that ZZW-115 treatment induced cell

death by apoptosis and necroptosis mechanisms, with a concomitant mitochondrial metabolism failure that triggers lower production of ATP. Furthermore, the ATP depletion cannot be rescued by the apoptosis inhibitor Z-VAD-FMK and/or the necrosis inhibitor Necrostatin-1, indicating that ZZW-115 induces cell death through the mitochondrial failure and the resulting ATP decrease. Our study demonstrated that ZZW-115, as a NUPR1 inhibitor, is a highly potential drug candidate for treating HCC.

ACKNOWLEDGMENTS

This work was supported by La Ligue Contre le Cancer, INCa, Canceropole PACA and INSERM to JI; Fondation de France to PSC; China Scholarship Council (to WL and CH); Programme XU GUANGQI to YX and JI; National Natural Science Foundation of China (81502920), the Fundamental Research Funds for the Central Universities (106112017CDJQJ468823) to YX and in part by the Associazione Italiana per la Ricerca sul Cancro (AIRC; project n. 18394) to MC.

Conflict of interest

Authors declare not conflicts of interest

REFERENCES

[1] G. Augello, M.R. Emma, A. Cusimano, A. Azzolina, S. Mongiovi, R. Puleio, G. Cassata, A. Gulino, B. Belmonte, R. Gramignoli, S.C. Strom, J.A. McCubrey, G. Montalto, M. Cervello, Targeting HSP90 with the small molecule inhibitor AUY922 (luminespib) as a treatment strategy against hepatocellular carcinoma, International journal of cancer, 144 (2019) 2613-2624.

[2] Y. Bak, H.J. Shin, I. Bak, D.Y. Yoon, D.Y. Yu, Hepatitis B virus X promotes hepatocellular carcinoma development via nuclear protein 1 pathway, Biochemical and biophysical research communications, 466 (2015) 676-681.

[3] C. Botto, G. Augello, E. Amore, M.R. Emma, A. Azzolina, G. Cavallaro, M. Cervello, M.L. Bondi, Cationic Solid Lipid Nanoparticles as Non Viral Vectors for the Inhibition of Hepatocellular Carcinoma Growth by RNA Interference, Journal of biomedical nanotechnology, 14 (2018) 1009-1016.

[4] J. Bruix, L.G. da Fonseca, M. Reig, Insights into the success and failure of systemic therapy for hepatocellular carcinoma, Nature reviews. Gastroenterology & hepatology, 16 (2019) 617-630.

[5] J. Bruix, M. Sherman, J.M. Llovet, M. Beaugrand, R. Lencioni, A.K. Burroughs, E. Christensen, L. Pagliaro, M. Colombo, J. Rodes, E.P.o.E.o. HCC, Clinical management of hepatocellular carcinoma. Conclusions of the Barcelona-2000 EASL conference. European Association for the Study of the Liver, Journal of hepatology, 35 (2001) 421-430.

[6] C.Y. Chen, S.M. Wu, Y.H. Lin, H.C. Chi, S.L. Lin, C.T. Yeh, W.Y. Chuang, K.H. Lin, Induction of nuclear protein-1 by thyroid hormone enhances platelet-derived growth factor A mediated angiogenesis in liver cancer, Theranostics, 9 (2019) 2361-2379.

[7] M.H. Chen, W.L. Yang, K.T. Lin, C.H. Liu, Y.W. Liu, K.W. Huang, P.M. Chang, J.M. Lai, C.N. Hsu, K.M. Chao, C.Y. Kao, C.Y. Huang, Gene expression-based chemical genomics identifies potential therapeutic drugs in hepatocellular carcinoma, PloS one, 6 (2011) e27186.

[8] A. de Conti, K. Dreval, V. Tryndyak, O.E. Orisakwe, S.A. Ross, F.A. Beland, I.P. Pogribny, Inhibition of the Cell Death Pathway in Nonalcoholic Steatohepatitis (NASH)-Related Hepatocarcinogenesis Is Associated with Histone H4 lysine 16 Deacetylation, Molecular cancer research : MCR, 15 (2017) 1163-1172.

[9] M.R. Emma, J.L. Iovanna, D. Bachvarov, R. Puleio, G.R. Loria, G. Augello, S. Candido, M. Libra, A. Gulino, V. Cancila, J.A. McCubrey, G. Montalto, M. Cervello, NUPR1, a new target in liver cancer: implication in controlling cell growth, migration, invasion and sorafenib resistance, Cell death & disease, 7 (2016) e2269.

[10] A. Forner, J.M. Llovet, J. Bruix, Hepatocellular carcinoma, Lancet, 379 (2012) 1245-1255.

[11] H. Huang, Y. Zhang, X. Wang, X. Zhou, S. Li, M. Wang, J. Ren, [Nuclear protein 1 knockdown inhibits proliferation and migration of HepG2 cells], Xi bao yu fen zi mian yi xue za zhi = Chinese journal of cellular and molecular immunology, 31 (2015) 782-786.

[12] Y. Ji, Z. Wang, H. Chen, L. Zhang, F. Zhuo, Q. Yang, Serum from Chronic Hepatitis B Patients Promotes Growth and Proliferation via the IGF-II/IGF-IR/MEK/ERK Signaling Pathway in Hepatocellular Carcinoma Cells, Cellular physiology and biochemistry : international journal of experimental cellular physiology, biochemistry, and pharmacology, 47 (2018) 39-53.

[13] Y.K. Lee, B.A. Jee, S.M. Kwon, Y.S. Yoon, W.G. Xu, H.J. Wang, X.W. Wang, S.S. Thorgeirsson, J.S. Lee, H.G. Woo, G. Yoon, Identification of a mitochondrial defect gene signature reveals NUPR1 as a key regulator of liver cancer progression, Hepatology, 62 (2015) 1174-1189.

[14] Y.K. Lee, H.G. Woo, G. Yoon, Mitochondrial defect-responsive gene signature in liver-cancer progression, BMB reports, 48 (2015) 597-598.

[15] J.L. Neira, J. Bintz, M. Arruebo, B. Rizzuti, T. Bonacci, S. Vega, A. Lanas, A. Velazquez-Campoy, J.L. Iovanna, O. Abian, Identification of a Drug Targeting an Intrinsically Disordered Protein Involved in Pancreatic Adenocarcinoma, Scientific reports, 7 (2017) 39732.

[16] P. Nicotera, G. Melino, Regulation of the apoptosis-necrosis switch, Oncogene, 23 (2004) 2757-2765.

[17] N. Pedrola, L. Devis, M. Llaurado, I. Campoy, E. Martinez-Garcia, M. Garcia, L. Muinelo-Romay, L. Alonso-Alconada, M. Abal, F. Alameda, G. Mancebo, R. Carreras, J. Castellvi, S. Cabrera, A. Gil-

Moreno, X. Matias-Guiu, J.L. Iovanna, E. Colas, J. Reventos, A. Ruiz, Nidogen 1 and Nuclear Protein 1: novel targets of ETV5 transcription factor involved in endometrial cancer invasion, Clinical & experimental metastasis, 32 (2015) 467-478.
[18] P. Santofimia-Castano, B. Rizzuti, Y. Xia, O. Abian, L. Peng, A. Velazquez-Campoy, J.L. Iovanna, J.L. Neira, Designing and repurposing drugs to target intrinsically disordered proteins for cancer treatment: using NUPR1 as a paradigm, Molecular & cellular oncology, 6 (2019) e1612678.
[19] P. Santofimia-Castano, Y. Xia, W. Lan, Z. Zhou, C. Huang, L. Peng, P. Soubeyran, A. Velazquez-Campoy, O. Abian, B. Rizzuti, J.L. Neira, J. Iovanna, Ligand-based design identifies a potent NUPR1 inhibitor exerting anticancer activity via necroptosis, The Journal of clinical investigation, 129 (2019) 2500-2513.
[20] S.M. Wilhelm, L. Adnane, P. Newell, A. Villanueva, J.M. Llovet, M. Lynch, Preclinical overview of sorafenib, a multikinase inhibitor that targets both Raf and VEGF and PDGF receptor tyrosine kinase signaling, Molecular cancer therapeutics, 7 (2008) 3129-3140.
[21] J.D. Yang, P. Hainaut, G.J. Gores, A. Amadou, A. Plymoth, L.R. Roberts, A global view of hepatocellular carcinoma: trends, risk, prevention and management, Nature reviews. Gastroenterology & hepatology, 16 (2019) 589-604.

Table 1. Demographic features and clinical parameters of the patients

	All (n=24)	Control (n=6)	CH (n=6)	LC (n=6)	HCC (n=6)
Age (years; median and range)	53 (38-69)	50.2 (42-64)	42.5 (38-58)	52 (44-66)	66.5 (64-69)
Gender n (%)					
Female	10 (41.6)	4 (66.7)	3 (50)	2 (33.3)	1 (16.7)
Male	14 (58.4)	2 (33.3)	3 (50)	4 (66.7)	5 (83.3)
ALT (IU/L; median and range)		19 (12-36)	39.5 (20-173)	62.5 (54-203)	31 (22-44)
AST (IU/L; median and range)		16 (14-30)	32 (25-106)	90.5 (52-197)	42 (22-53)
Child Pugh Class n (%)					
A				6 (100)	6 (100)
B				-	-
C				-	-
MELD (mean ± SD)				10.6±1.5	9.5±0.5
TNM n (%)					
Stage 1					4 (66.7)
Stage 2					2 (33.3)
Stage 3					-
Stage 4					-
BCLC n (%)					
0					-
A					4 (66.7)
B					2 (33.3)
C					-
D					-

ALT: Alanine Aminotransferase

AST: Aspartate Aminotransferase

MELD: Score MELD (Model for End-Stage Liver Disease)

BCLC: Barcelona Clinic Liver Cancer staging

FIGURE LEGENDS

Figure 1

NUPR1 increased its expression according to the liver diseases. (A) Immunohistochemical staining of NUPR1 on sections of healthy human liver tissue and in samples from patients with diagnosis of hepatitis, cirrhosis and HCC was performed. A representative picture of each group is shown. (B) Quantification of percentage of NUPR1 positive and negative cells in the samples was done. The percentage of NUPR1 positive or negative cell was calculated as the ratio of staining cells to total cells in random fields (n=6). For each group, statistical significance is *** $P < 0.001$, **** (1-way ANOVA, Tukey's post hoc test). (C) Differential NUPR1 expression levels among peritumoral tissue (n=50) and primary HCC (n=371). (D) Kaplan–Meier Overall Survival for HCC patients in the TCGA cohort based in NUPR1 levels.

Figure 2

HCC derived cell lines, HepG2 and Hep3B, are sensitive to ZZW-115 treatment. Chemogram assays were done on HepG2 and Hep3B cell lines with increasing concentrations of ZZW-115 (n=3). IC_{50} and the area under the curve (AUC) values were calculated from integration of the viability curves by GraphPad Prism software.

Figure 3

ZZW-115 inhibits the growth of HepG2 and Hep3B cells xenografted in mice by apoptosis. (A) CAnN.Cg-Foxn1nu/Crl BALB/c nude mice xenografted with HepG2 cells were separated into 3 groups of 5 mice and treated daily for 20 days with 0.5% DMSO in physiologic serum (control group) or 5 or 2.5 mg/kg ZZW-115 compound. Mean of the volume of each treatment and individual volume of each mouse are shown. (B) Two groups of 5 Hep3B tumor-bearing mice were treated with 0.5% DMSO or with 5 mg/kg ZZW-115. Tumor growth curves are represented as individual volume of each mouse or as the mean of the group. Representative pictures of mice from control and 5 mg/kg ZZW-115 groups are shown. Data represent mean ± SEM, n = 5. For all statistical analysis: ** $P < 0.01$; *** $P < 0.001$. (C) Immunostaining of Ki67 and cleaved Caspase-3 on tumor sections of tumors from mice treated with 0.5% DMSO or 5 mg/kg ZZW-115 are shown. (D) Quantification of immunofluorescence staining of Ki67 and cleaved Caspase-3 are shown in representative pictures (n=3). Data represent mean ± SEM and were analyzed using the Student's t test; **** $P < 0.0001$.

Figure 4

ZZW-115 promoted apoptosis and necrosis and can be reverted by Z-VAD-FMK and Necrostatin-1. (A) HepG2 and Hep3B cells were pretreated with 20 µM Z-VAD-FMK and/or 40 µM Necrostatin-1 and subsequently treated with 2 µM of ZZW-115 for HepG2 and 3 µM for Hep3B for 18 h. Flow cytometry analysis of Annexin V and PI staining following at the end of the treatment was performed. A representative experiment of the dot plot profile of cells is shown (n = 3). (B) Quantitative analysis of AnnexinV and PI positive cells was done. Data represent mean ± SEM and were analyzed using 1-way ANOVA, Tukey's post hoc test (C) HepG2 and Hep3B cells were pre-treated with 20 µM Z-VAD-FMK and/or 40 µM Necrostatin-1 in combination with 0, 4 or 6 µM of ZZW-115 for 24 h. (C) Caspase 3/7 activity and (E) LDH release were measured in HepG2 and Hep3B cells. Data represent mean ± SEM, n = 3. Statistical significance is *P < 0.05, ***P < 0.001, and **** P < 0.0001 (2-way ANOVA, Bonferroni's post hoc test).

Figure 5

ZZW-115 treatment induced a dose-dependent ATP depletion by abolishing OXPHOS metabolism and mitochondrial funtion in HepG2 cells. ATP content of the (A) HepG2 cells was quantified 24 h after incubation with increasing concentrations of ZZW-115 alone or in the presence of 20 µM Z-VAD-FMK and/or 40 µM Necrostatin-1. Data represent mean ± SEM, n = 3. (B) OXPHOS metabolism, reflected by the oxygen consumption rate (OCR) levels for basal respiration (B. resp.), maximal respiration (M. resp.), spare capacity (S. Cap.), and ATP production (ATP prod.) were measured after 8 (A) or 24 (B) hours of treatment with 0.5 µM. (C) Mitochondrial membrane potential was quantified after 24 hours of incubation with increasing concentrations of ZZW-115. Data represent mean ± SEM and were analyzed using 1-way ANOVA, Tukey's post hoc test. (D) ADP/ATP ratio was measured at increasing concentration of ZZW-115 after 24 hours of treatment. (E) Anaerobic glycolytic metabolism reflected by extracellular acidification rate (ECAR) levels for glycolysis (Glyco.), glycolytic capacity (G. Cap.), and glycolysis reserve (G. Res.) were measured after 8 (E) or 24 (F) hours of treatment with 0.5 µM. Data represent mean ± SEM, n = 3. Statistical significance is *P < 0.05, **P < 0.01, ***P < 0.001, and **** P < 0.0001 (2-way ANOVA, Bonferroni's post hoc test).

Legend of Supplementary Figure 1

ZZW-115 treatment induced a dose-dependent ATP depletion by abolishing OXPHOS metabolism and mitochondrial funtion in Hep3B cells. ATP content of the (A) Hep3B cells was quantified 24 h after incubation with increasing concentrations of ZZW-115 alone or in the presence of 20 µM Z-VAD-FMK and/or 40 µM Necrostatin-1. Data represent mean ± SEM, n = 3. (B) OXPHOS metabolism, reflected by the oxygen consumption rate (OCR) levels for basal respiration (B. resp.), maximal respiration (M. resp.), spare capacity (S. Cap.), and ATP production (ATP prod.) were measured after 8 (A) or 24 (B) hours of treatment with 0.5 µM. (C) Mitochondrial membrane potential was quantified after 24 hours of incubation with increasing concentrations of ZZW-115. Data represent mean ± SEM and were analyzed using 1-way ANOVA, Tukey's post hoc test. (D) ADP/ATP ratio was measured at increasing concentration of ZZW-115 after 24 hours of treatment. (E) Anaerobic glycolytic metabolism reflected by extracellular acidification rate (ECAR) levels for glycolysis (Glyco.), glycolytic capacity (G. Cap.), and glycolysis reserve (G. Res.) were measured after 8 (E) or 24 (F) hours of treatment with 0.5 µM. Data represent mean ± SEM, n = 3. Statistical significance is *P < 0.05, **P < 0.01, ***P < 0.001, and **** P < 0.0001 (2-way ANOVA, Bonferroni's post hoc test).

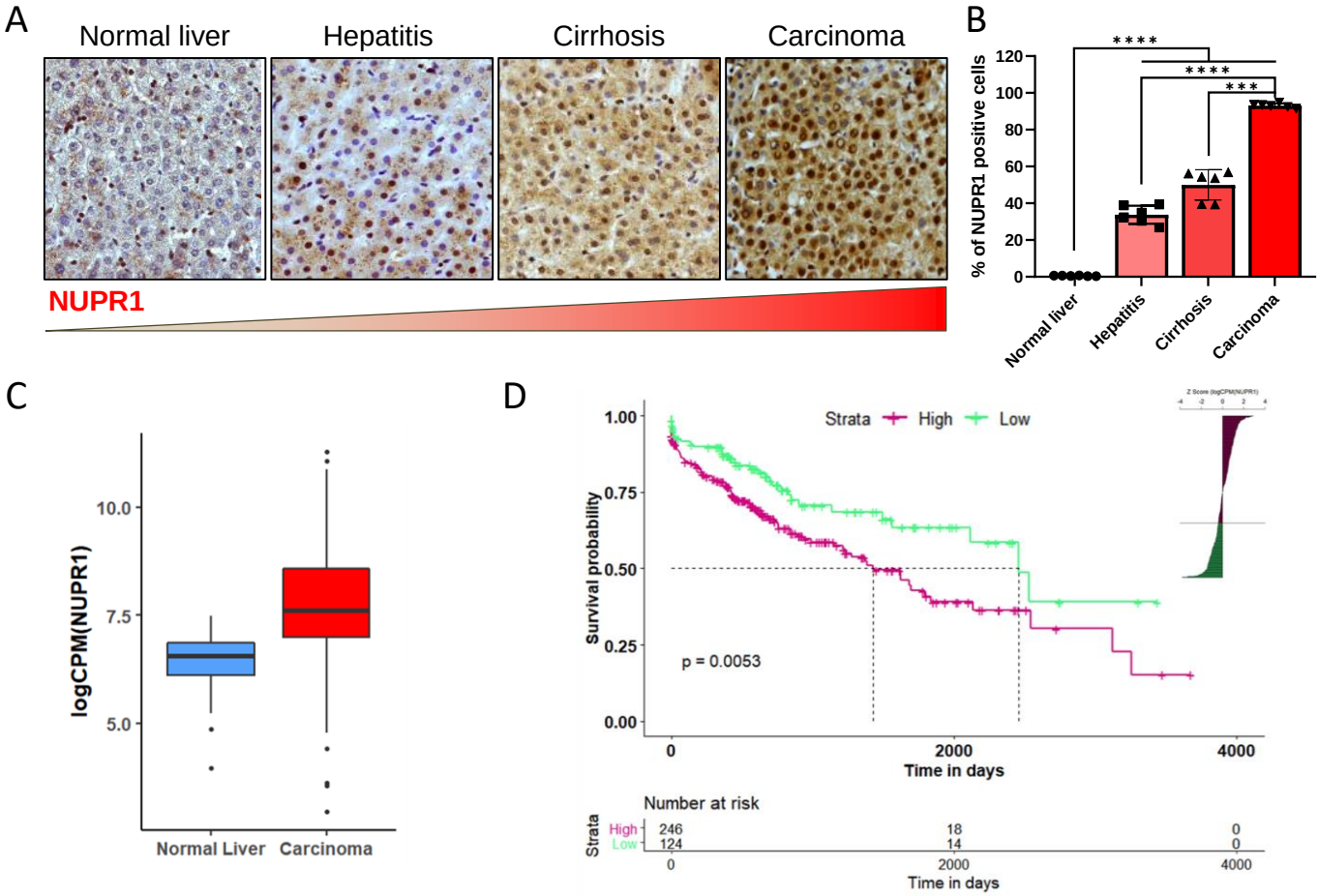
A
Normal liver
Hepatitis
Cirrhosis
Carcinoma
NUPR1
B
% of NUPR1 positive cells
120
100
80
60
40
20
0
****
****
***
Normal liver
Hepatitis
Cirrhosis
Carcinoma
C
logCPM(NUPR1)
10.0
7.5
5.0
Normal Liver
Carcinoma
D
Strata
High
Low
Survival probability
1.00
0.75
0.50
0.25
0.00
p = 0.0053
0
2000
4000
Time in days
Number at risk
Strata
High
Low
246
124
18
14
0
0
0
2000
4000
Time in days

Figure 1

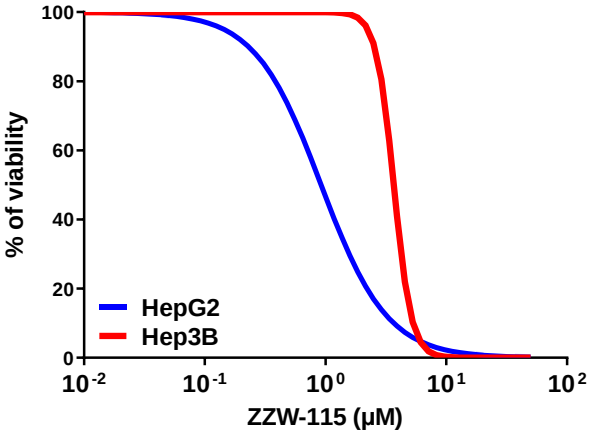

	HepG2	Hep3B
AUC	241.9 ± 8.63	420.4 ± 15.03
IC50 (μM)	0.97 ± 0.27	3.31 ± 0.40

Figure 2

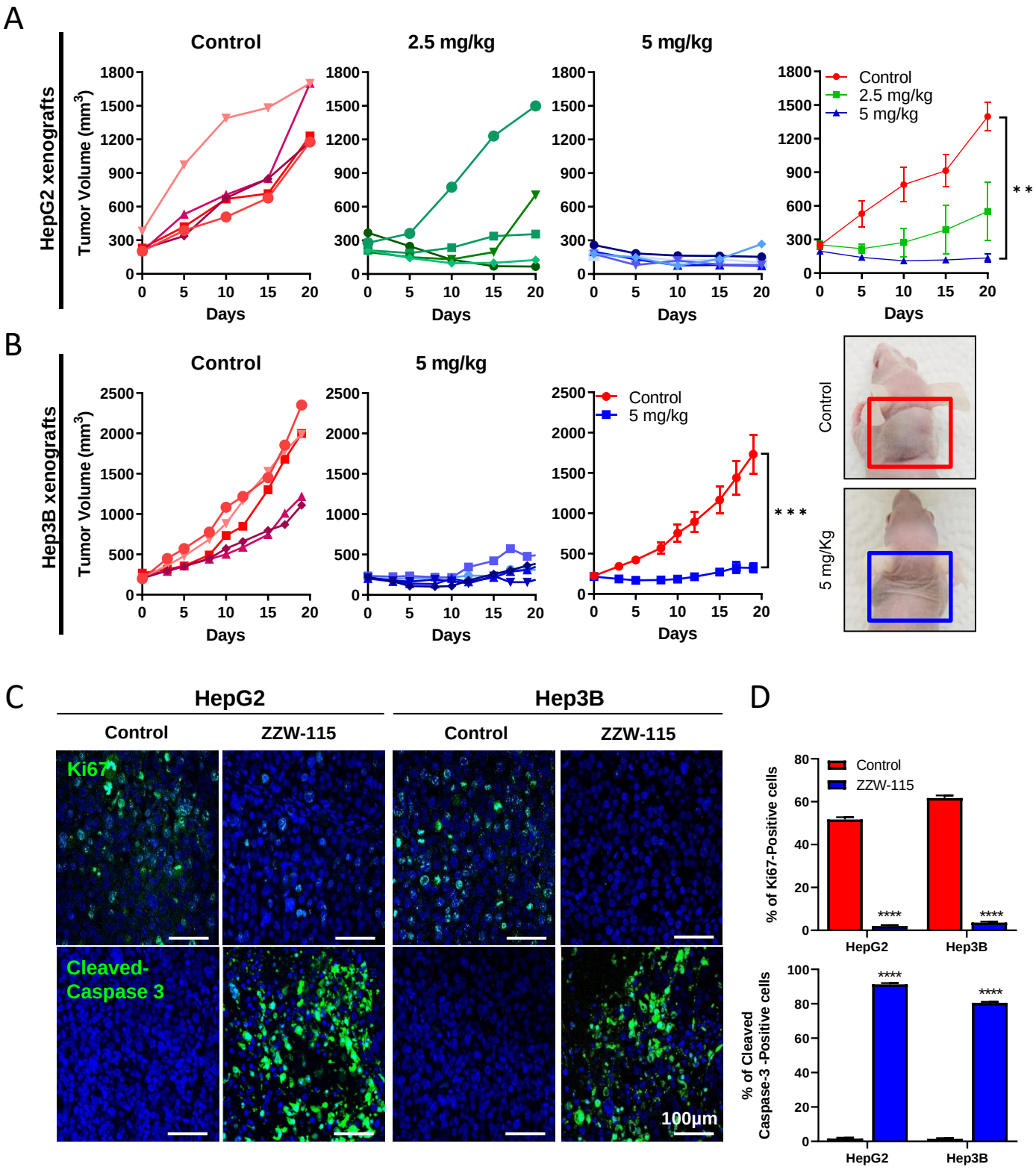
A
Control
2.5 mg/kg
5 mg/kg
HepG2 xenografts
Tumor Volume (mm3)
Days
Control
2.5 mg/kg
5 mg/kg
**
B
Control
5 mg/kg
Hep3B xenografts
Tumor Volume (mm3)
Days
Control
5 mg/kg
***
Control
5 mg/Kg
C
HepG2
Hep3B
Control
ZZW-115
Control
ZZW-115
Ki67
Cleaved-
Caspase 3
100μm
D
Control
ZZW-115
% of Ki67-Positive cells
****
HepG2
Hep3B
% of Cleaved
Caspase-3 -Positive cells
****
HepG2
Hep3B

Figure 3

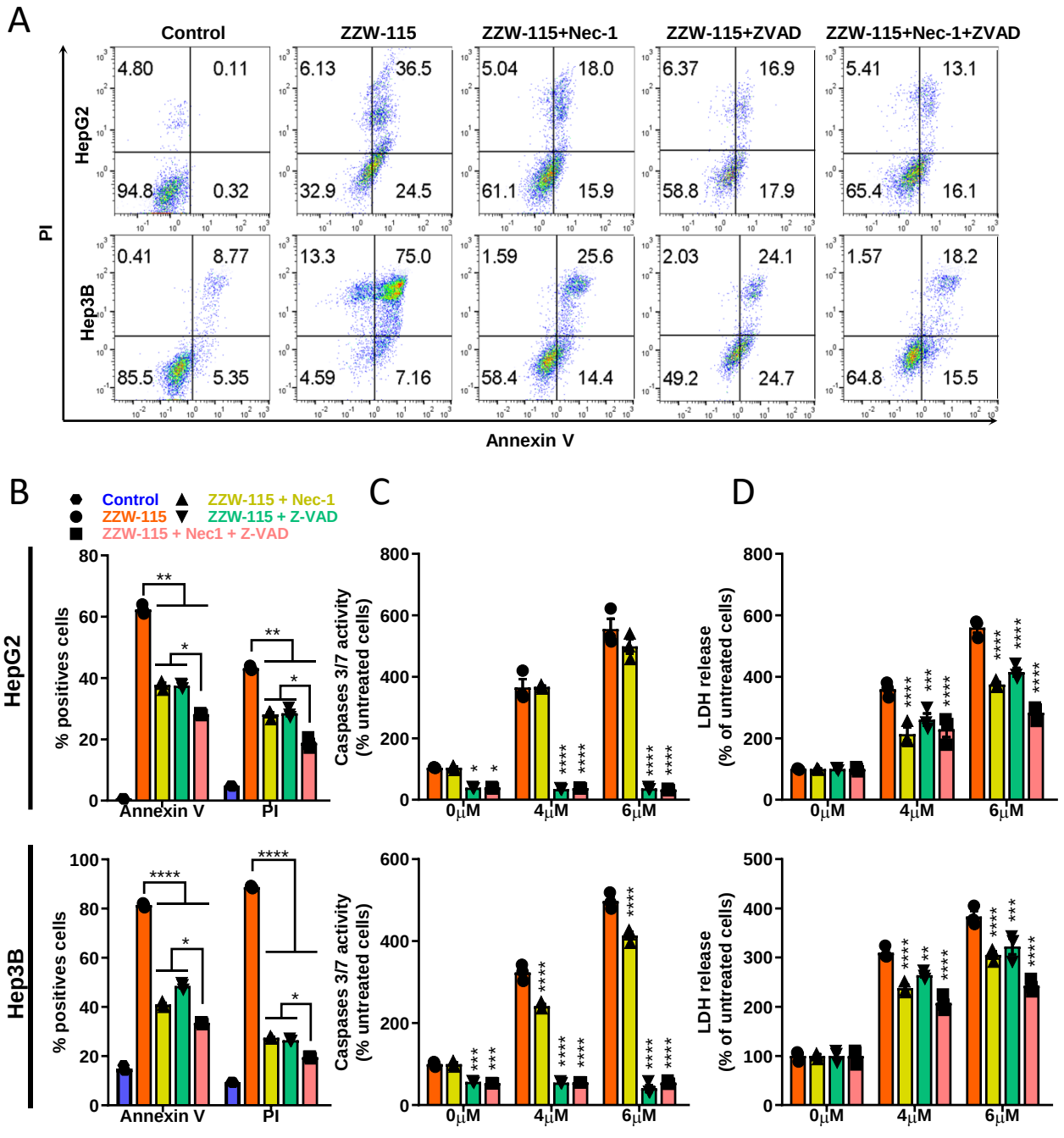
A
Control
ZZW-115
ZZW-115+Nec-1
ZZW-115+ZVAD
ZZW-115+Nec-1+ZVAD
HepG2
Hep3B
PI
Annexin V
4.80
0.11
94.8
0.32
6.13
36.5
32.9
24.5
5.04
18.0
61.1
15.9
6.37
16.9
58.8
17.9
5.41
13.1
65.4
16.1
0.41
8.77
85.5
5.35
13.3
75.0
4.59
7.16
1.59
25.6
58.4
14.4
2.03
24.1
49.2
24.7
1.57
18.2
64.8
15.5
B
C
D
Control
ZZW-115
ZZW-115 + Nec-1
ZZW-115 + Z-VAD
ZZW-115 + Nec1 + Z-VAD
HepG2
Hep3B
% positives cells
Annexin V
PI
Caspases 3/7 activity
(% untreated cells)
LDH release
(% of untreated cells)
0μM
4μM
6μM

Figure 4

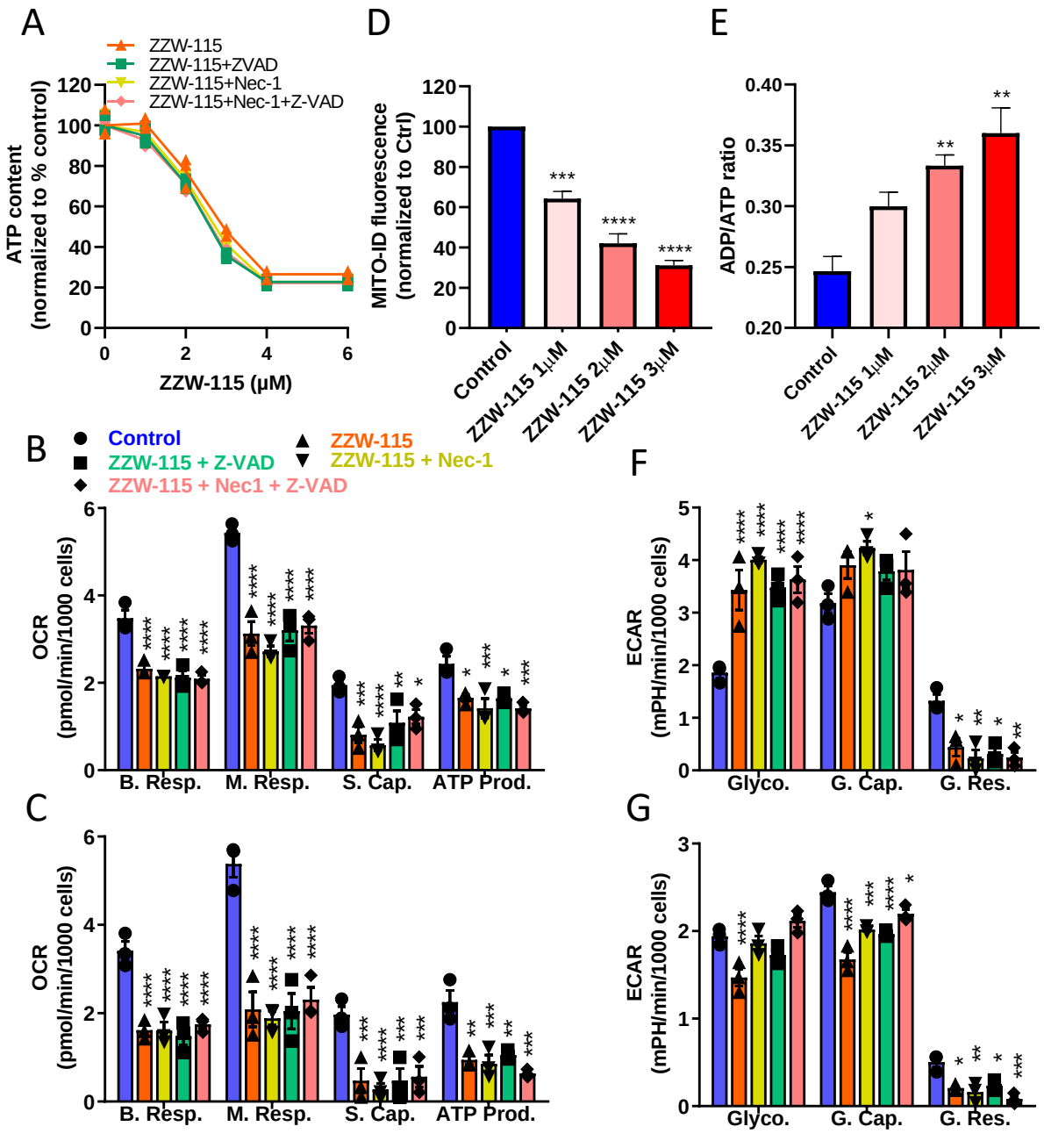
A
ZZW-115
ZZW-115+ZVAD
ZZW-115+Nec-1
ZZW-115+Nec-1+Z-VAD
ATP content (normalized to % control)
ZZW-115 (μM)
D
MITO-ID fluorescence (normalized to Ctrl)
Control
ZZW-115 1μM
ZZW-115 2μM
ZZW-115 3μM
E
ADP/ATP ratio
Control
ZZW-115 1μM
ZZW-115 2μM
ZZW-115 3μM
B
Control
ZZW-115
ZZW-115 + Z-VAD
ZZW-115 + Nec-1
ZZW-115 + Nec1 + Z-VAD
OCR (pmol/min/1000 cells)
B. Resp.
M. Resp.
S. Cap.
ATP Prod.
F
ECAR (mPH/min/1000 cells)
Glyco.
G. Cap.
G. Res.
C
OCR (pmol/min/1000 cells)
B. Resp.
M. Resp.
S. Cap.
ATP Prod.
G
ECAR (mPH/min/1000 cells)
Glyco.
G. Cap.
G. Res.

Figure 5